

Supplement of Atmos. Chem. Phys., 18, 12345–12361, 2018
<https://doi.org/10.5194/acp-18-12345-2018-supplement>
© Author(s) 2018. This work is distributed under
the Creative Commons Attribution 4.0 License.



Supplement of

Historical black carbon deposition in the Canadian High Arctic: a >250-year long ice-core record from Devon Island

Christian M. Zdanowicz et al.

Correspondence to: Christian M. Zdanowicz (christian.zdanowicz@geo.uu.se)

The copyright of individual parts of the supplement might differ from the CC BY 4.0 License.

Supplemental Information

Black Carbon - Continuous flow analysis (CFA)

Determination of rBC concentrations in the Devon Island DV99.1 ice core archive were performed within the Curtin University Trace Research Advanced Clean air facility (TRACE) using a continuous flow ice core melting system coupled to an intracavity laser-induced single particle incandescence soot photometer (Droplet Measurement Technologies). Sections of ice core used for the study were logged, measured and sectioned into square longitudinal samples of ice inside a class 100 walk-in freezer in the TRACE facility. The ends of samples were carefully scraped with a ceramic chisel blade and the samples relocated to a chest freezer next to the CFA melter system. The system is similar to the ice core melter system used by McConnell and Edwards (2008) with the exception that the melter head was made out of aluminium rather than silicon carbide. A schematic of the system is provided below (**Fig. S1**).

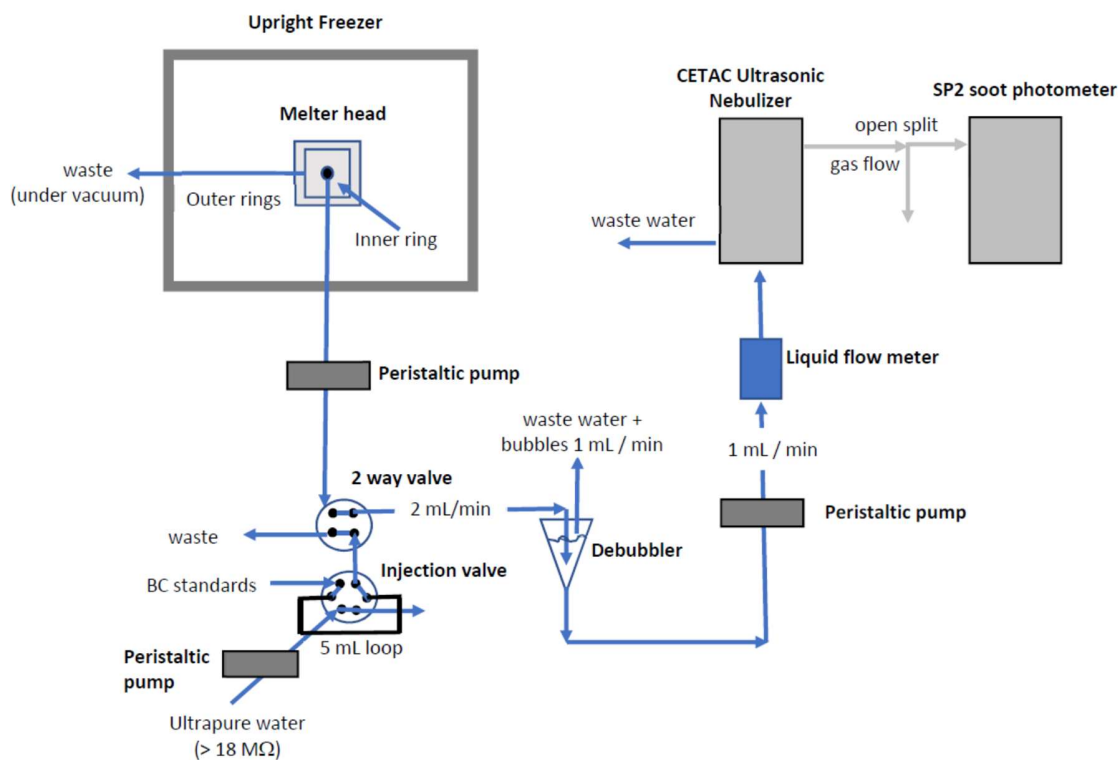


Figure S1: Schematic of the Continuous Flow Analysis (CFA) - SP2 system used for the analysis of the DV99.1 core at the Trace Research Clean Environmental facility, Curtin University.

The ice core sections were continuously loaded into the melter stand in sequence and melted at a rate of $\sim 3 \text{ cm min}^{-1}$. Only melt water from the inner most ring of the melter head was used for the study. From the inner ring, melt water containing bubbles of air (from the ice core) was pumped through Teflon PFA capillary lines (inner diameter 0.3 in, or 7.62 mm), by a peristaltic pump, into a 2-way four port valve (VICI) and a small debubbling system. The debubbling system was used to remove air bubbles from the

line and to decouple the liquid flow from the ice core melter to the ultrasonic nebulizer and desolvation system. The 4-port valve was used to select ice core melter flow or rBC standards and/or ultrapure water via a 2-way, 6-port injection valve (VICI). The injection loop was ~5 mL. Debubbled water flowing into the ultrasonic nebulizer (U5000AT; CETAC Technologies, Omaha, NE, USA) was measured using an inline water flow meter (Truflo, Glass Expansion). The efficiency of the nebulizer was evaluated by weighing water pumped from the systems primary waste line. The nebulizer efficiency (~25%, defined as the percent mass of water aerosol exiting the nebulizer chamber in to the heated section) was monitored gravimetrically to check the nebulizer stability. Instrumental settings are shown in **Table S1**.

SP2 settings	
Sample gas flow rate	120 cm ³ min ⁻¹
Sheat gas flow rate	1000 cm ³ min ⁻¹
Purge gas flow rate	276 cm ³ min ⁻¹
Laser power setting	4.1
Nebulizer settings	
Gas flow rate	980 cm ³ min ⁻¹
Liquid flow rate	1013 μL min ⁻¹

Table S1. Instrumental settings for the SP2 and nebulizer used in this study.

The colloidal BC standards used for the study were derived from a commercially available 100% carbon black pigment (MIS, Eboni-6-4K, dispersed in water). This material was used in preference to the standards used by McConnell et al. (2007) because of its larger particle size, which is closer to the geometric mean volume equivalent diameter (~200 nm) of BC found in the remote atmosphere. Electron microscope images of the standard rBC particles are shown in **Fig S2**. Thermogravimetric analysis of the standard revealed the dry mass to be 7.06% of the liquid mass. The dry mass was stable in air from 200 to 400°C. We have recently analysed a fresh batch of the same pigment and found a comparable dry mass of 7.23% at 400°C (for 40 min in air). After increasing the temperature to 480° C (for 40 min) the material glowed red with no visible emissions suggesting an autoignition temperature between 400 and 480°C. The temperature was increased to a final temperature of 580 °C for 40 min. We found no mass change between the 480°C and 580°C stage. The remaining mass after the 580°C stage was 7.3% of the dry mass. Based on the thermogravimetric analysis we concluded that 92.7% of the dry mass at 400 C was rBC. Concentration standards were prepared by serial dilution of the pigment with ultrapure water based on the results of the thermogravimetric analysis.

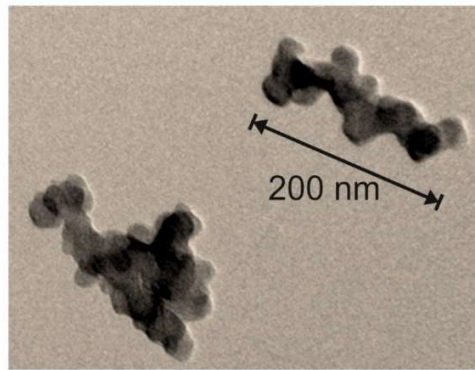


Figure S2: Transmission Electron Microscope image of colloidal carbon black pigment particles (MIS EB6-4K) used as standards for calibration of the SP2.

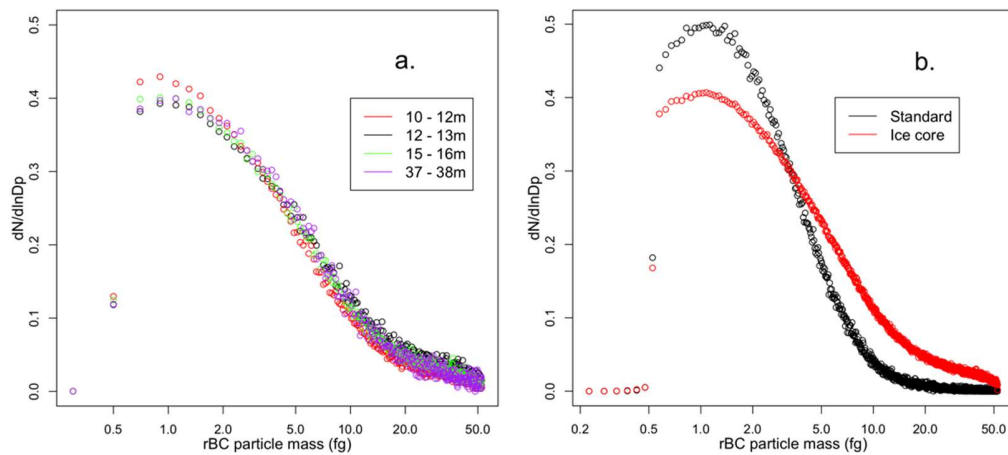


Figure S3: rBC normalised probability distributions of rBC mass determined with the SP2 as a function of particle mass: **(a)** Ice core sections spanning depths 10–12 m, 12–13 m, 15–16 m, and 37–38 m. The 10–16 m sections are from years ~ 1943–1963, while the 37–38 m section is from years ~1803–1814; **(b)** MIS EB6-4K rBC standard (black) and the Devon ice core (red).

We investigated changes in the Devon ice core rBC mass distribution from preindustrial and industrial ice sections (**Fig. S3a**) and sections with significant infiltration ice layers (12 -13m and 15 – 16 m). We found no significant difference between the rBC mass distribution either between the preindustrial and industrial sections or between the sections with infiltration ice. The rBC mass concentration distribution for the external standard “MIS EB6-4K” and the ice core are shown in **Fig. S3b**. The ice core samples and the rBC standards used by the study were similar with respect to the mass concentration number peak. The probability distribution of rBC mass concentration in the DV99.1 ice core was however broader than in the standard (Fig. S3), with a rBC geometric mean mass of ~ 2.2 fg ($n = 1837437$) compared to the standard geometric mass of ~ 1.7 fg ($n = 333609$).

A typical calibration sequence, run at the beginning and at the end of the melt sequence is shown in **Fig. S4a**. The linear calibration is shown in **Fig. S4b**, and incorporates both the standard sequence run at the beginning and at the end of the day's melt sequence, ~5 hours apart. The response of standards run during pauses (**Fig. S4c**) in the melting were relatively stable (relative standard deviation < 8%).

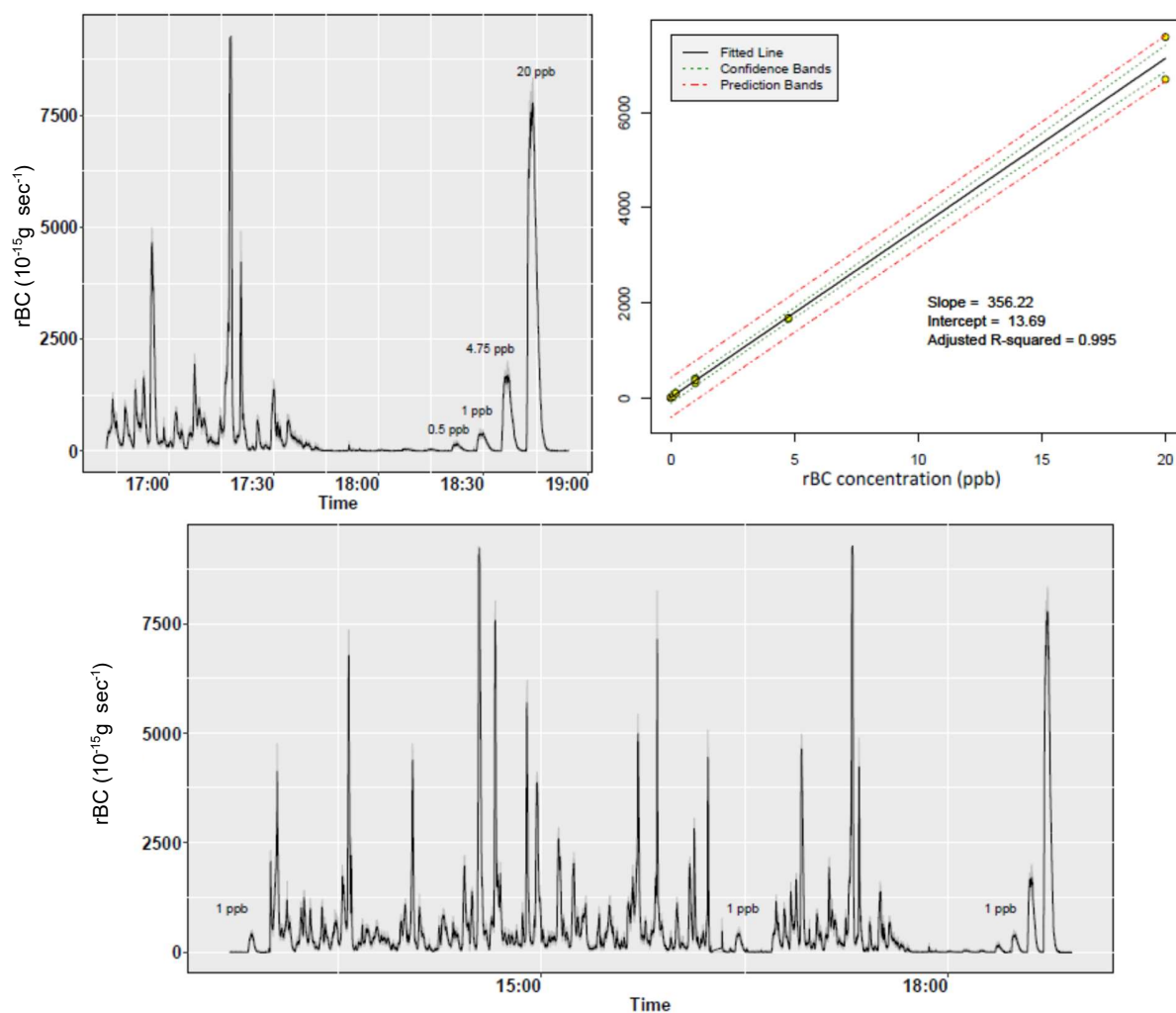


Figure S4: rBC external calibration for 10 Dec., 2012. **(a)** Calibration sequence at the end of the melt run; **(b)** linear calibration comprising all of the day's standards; **(c)** plot showing 1 ng g⁻¹ (ppb) rBC external standards run during pauses in the core melting sequence. The y axis units for all panels are fg rBC sec⁻¹ which is equivalent to fg rBC per 2 sccm of air.

Analyses were conducted over the course of five days (5-11 Dec., 2012) with the same set of standards. The sensitivity of the analytical system remained stable on 6-7 Dec. with linear calibration slopes of ~ 434 and 444, respectively. However the calibration slopes from 10-11 Dec. were 356 and 360, respectively. This step in sensitivity is related to a change within the SP2 instrument and not due to aggregation of the standard. While the change in slope is roughly 19 %, the rBC concentrations either side of the step in sensitivity were essentially the same (**Fig. S5 & S6**) and no change in the rBC mass distribution was found.

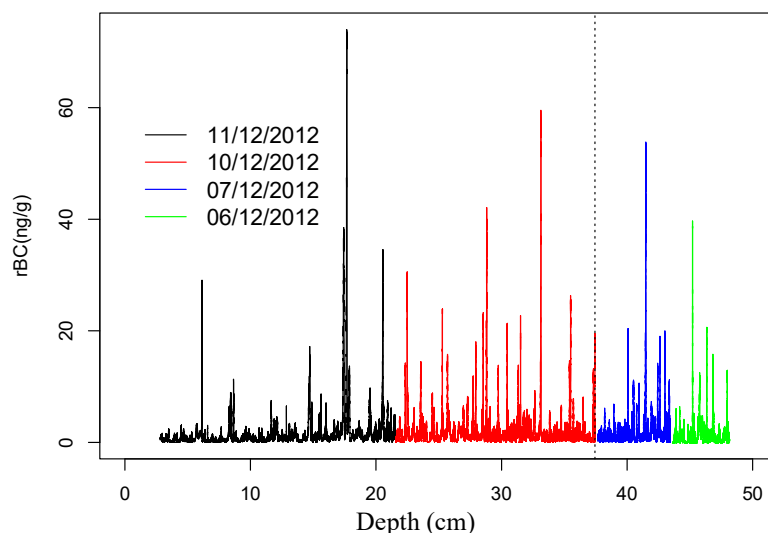


Figure S5. rBC concentrations versus depth highlighting ice core analysis date. The dashed vertical line marks the shift in calibration slope.

For example the geometric mean rBC concentration was 0.773 ng g^{-1} ($n = 2618$) for depths 37.68 to 39.00 m (determined on 7 Dec.) and 0.722 ng g^{-1} ($n = 2671$) for depths 37.44 to 36.00 m (determined on 10 Dec.). For depths 37.00 to 37.44 m the geometric mean rBC concentration was 0.656 ng g^{-1} ($n = 1301$, from 10 Dec.) and for depths 37.68 to 38.31 m it was 0.661 ng g^{-1} ($n = 1310$, from 7 Dec.). Since the difference between the ice sections bridging the sensitivity shift is $< 2\%$ we conclude that the SP2 instrument / desolvation system sensitivity dropped and that the external standards remained constant in colloidal mass concentration.

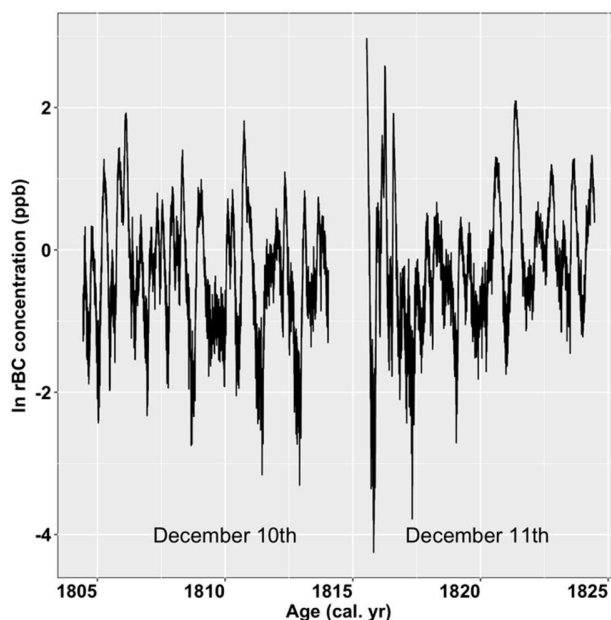


Figure S6. Comparison of rBC concentrations determined on 7 and 10 December, 2012. The data are plotted on a logarithmic scale to better compare the geometric mean concentrations.

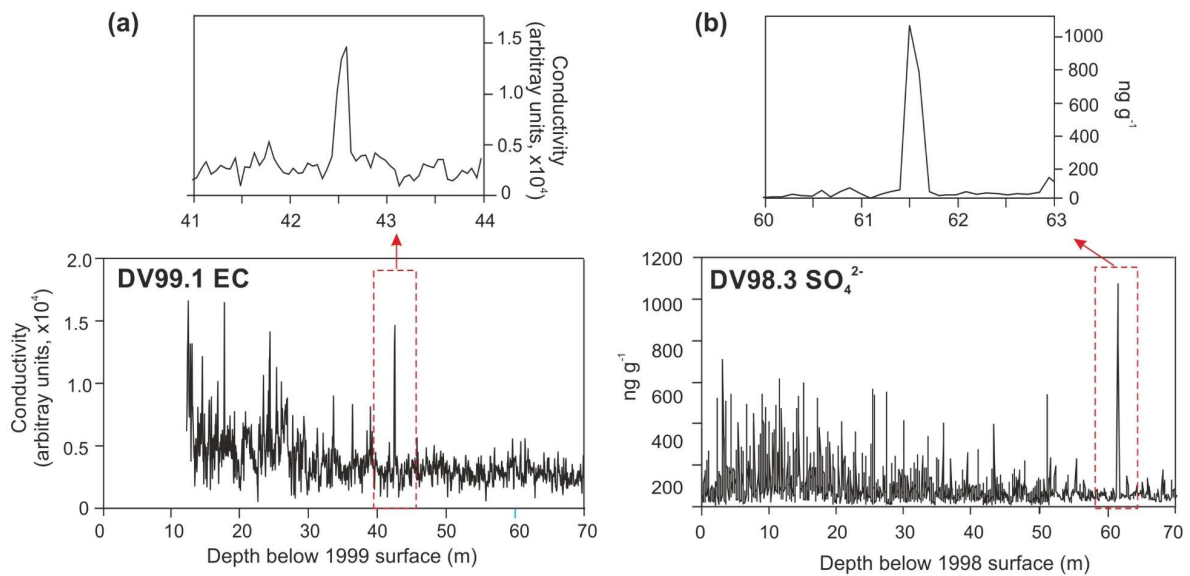


Figure S7: Profiles of EC in the DV99.1 core (a; profile starts at 12.4 m) and of SO_4^{2-} concentrations in the DV98.3 core (b) down to 70 m depth. Enlargements above each plot show peaks in these profiles that were ascribed to fallout from the Laki 1783 eruption, and were used to correlate the two cores.

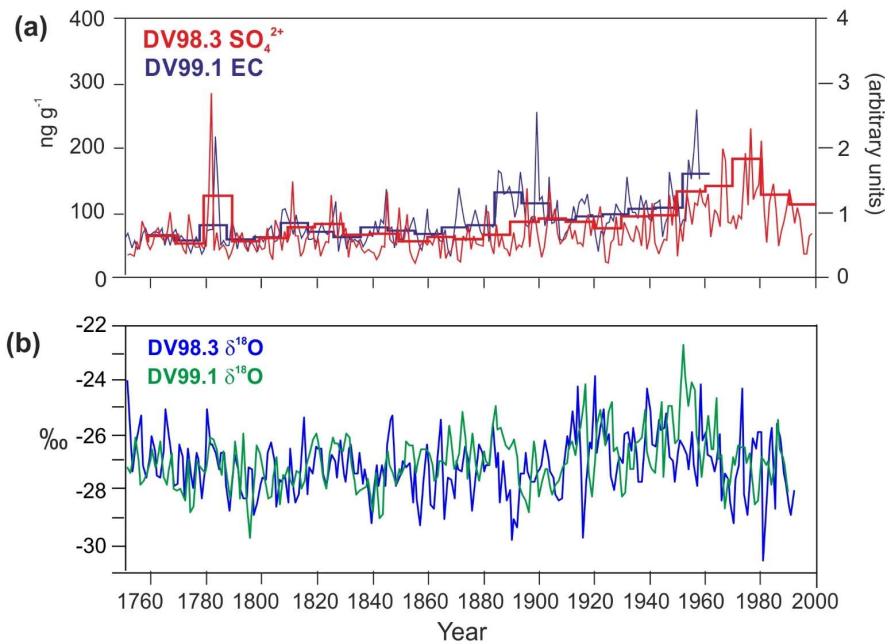


Figure S8: (a) The DV99.1 record of EC (right-hand scale) overlaid on the DV98.3 record of SO_4^{2-} concentrations (left-hand scale) over the period 1740-1998. Data are shown in averages of \sim one year (thinner lines) and \sim 10 years (bolder, stepped lines), the latter starting with the last year in each record. (b) Overlaid $\delta^{18}\text{O}$ records from the DV99.1 and DV98.3, averaged over intervals of \sim one year. On this figure, the mean $\delta^{18}\text{O}$ of the DV99.1 record was offset by -2.2‰ to show the degree of matching between the two records. See also next figure.

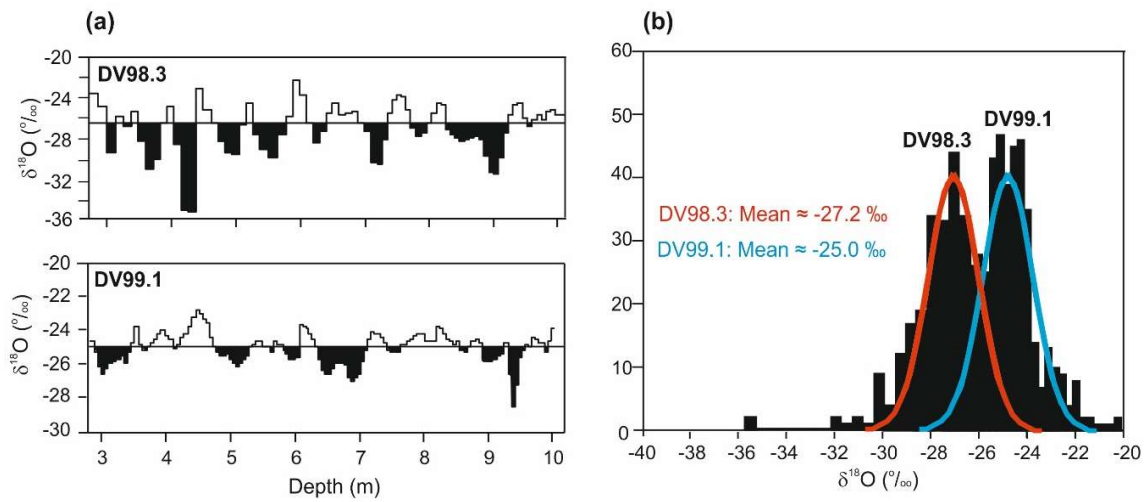


Figure S9: (a) Compared $\delta^{18}\text{O}$ profiles in two shallow sections of the DV98.3 and DV99.1 cores from Devon ice cap, showing the attenuation of seasonal variations in the DV99.1 core relative to the DV98.3 core. (b) Overlaid histograms of $\delta^{18}\text{O}$ values in the core sections shown in (a), with Gaussian models fitted to each.

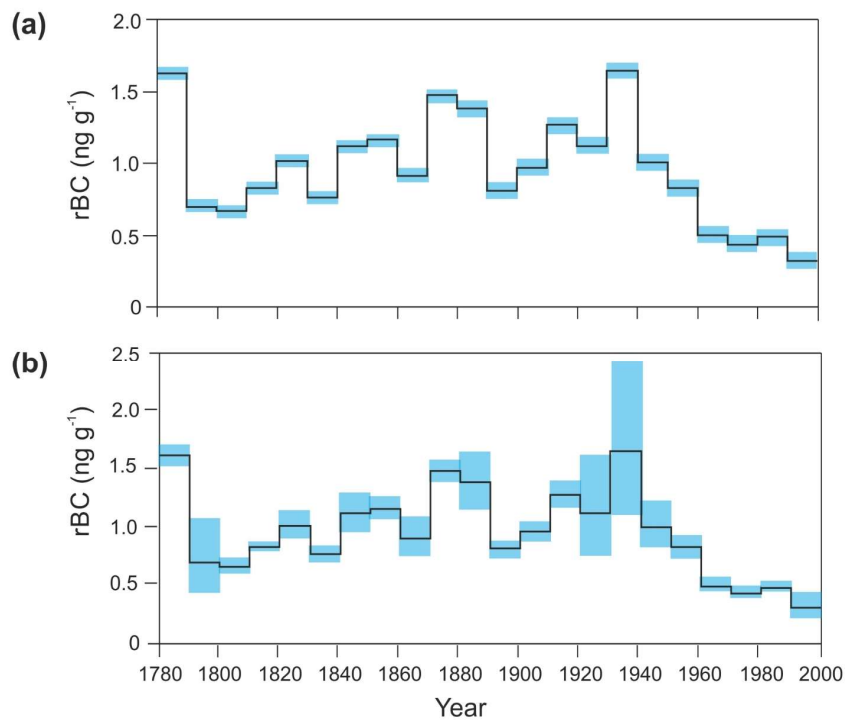


Figure S10: Uncertainties on 10-year averages (geometric mean) of rBC concentrations in the DV99.1 core over the period 1780-2000 arising from various error sources, and estimated by Monte Carlo methods. (a) Uncertainties arising from spatial variability of rBC deposition across the summit area of Devon ice cap. (b) Uncertainties arising from potential errors in the age model used for the DV99.1 core. The range of uncertainties for any decade in the rBC data is shown as blue shading bounded by 95 % confidence limits (CL). Note that the estimated mean rBC concentration in the last decade (1990-2000) is based on ~2 years of data only.

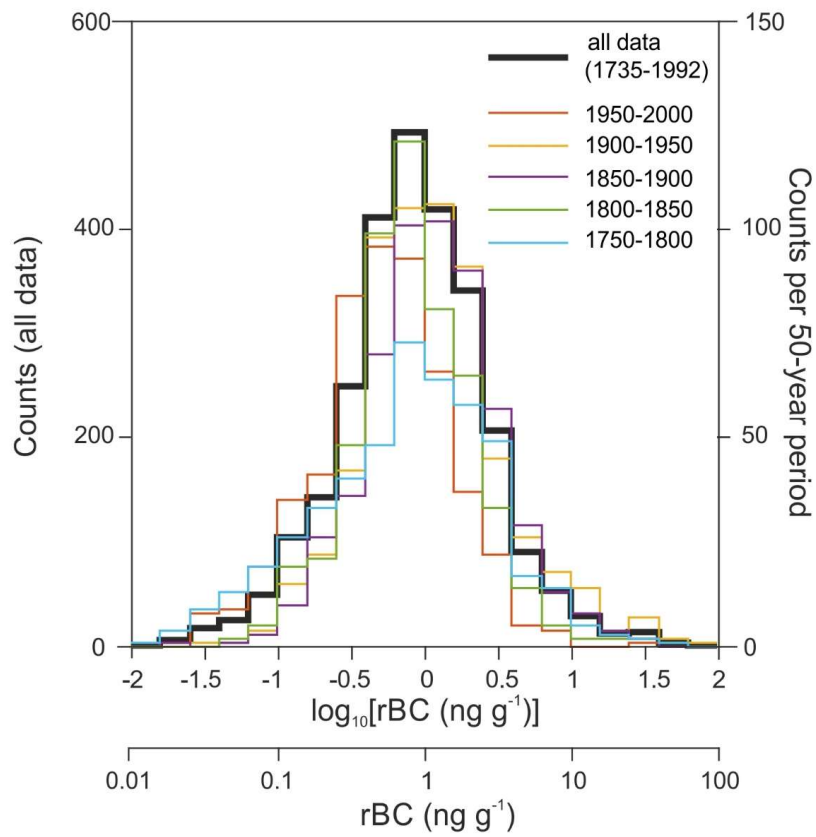


Figure S11: Probability distribution of rBC concentrations measured in the DV99.1 core. The bold dark line includes all data (scale at left), while the coloured lines include data over discrete 50-year intervals (scale at right).

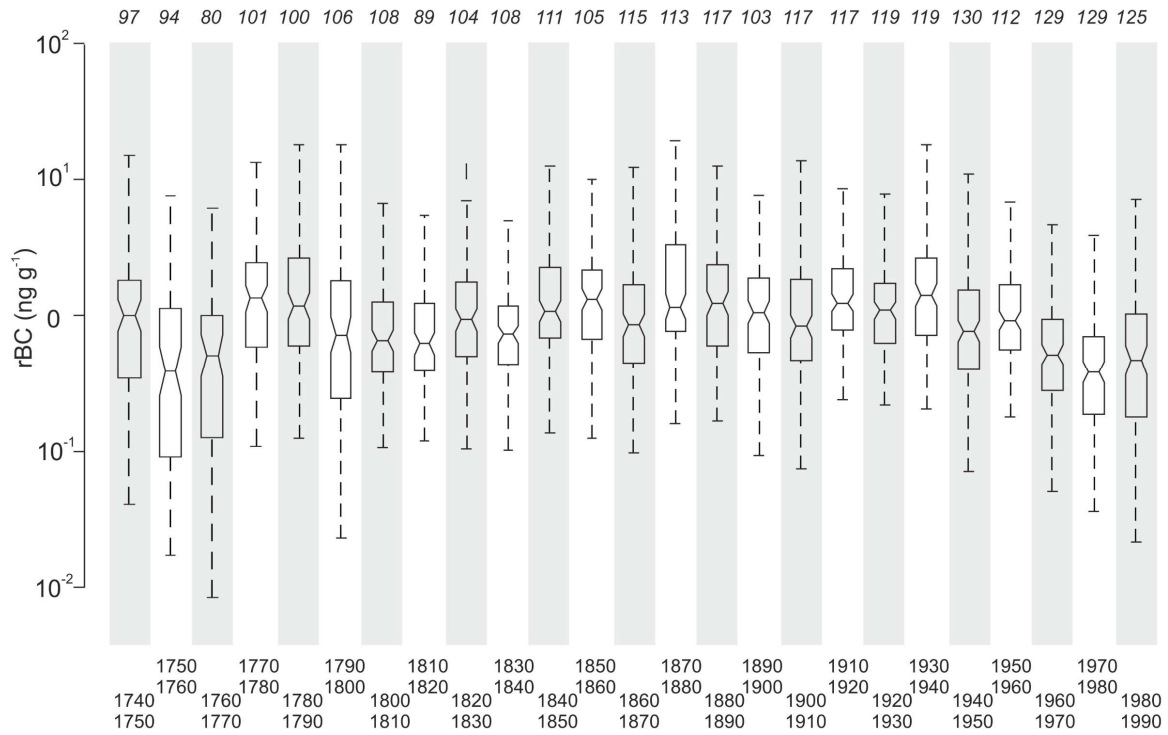


Figure S12: Notched box plots of rBC concentrations in the DV99.1 core, grouped by estimated decadal intervals from 1740 to 1990. Figures in italics at top of plot are the number of data points included in each decadal interval. Notches in the box plots denote the 95 % confidence intervals of the estimated median concentration in each decade.

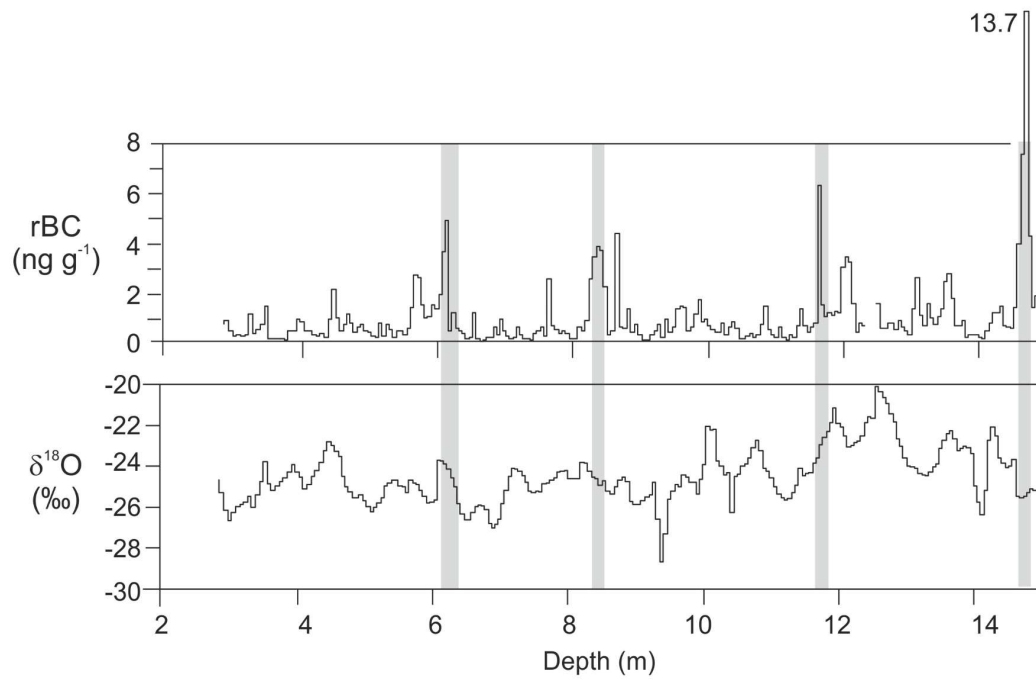


Figure S13: Variations of rBC concentrations and $\delta^{18}\text{O}$ measured in the uppermost 14.5 m of the DV99.1 core. Some of the most outstanding peaks in rBC concentrations are highlighted by grey shading.

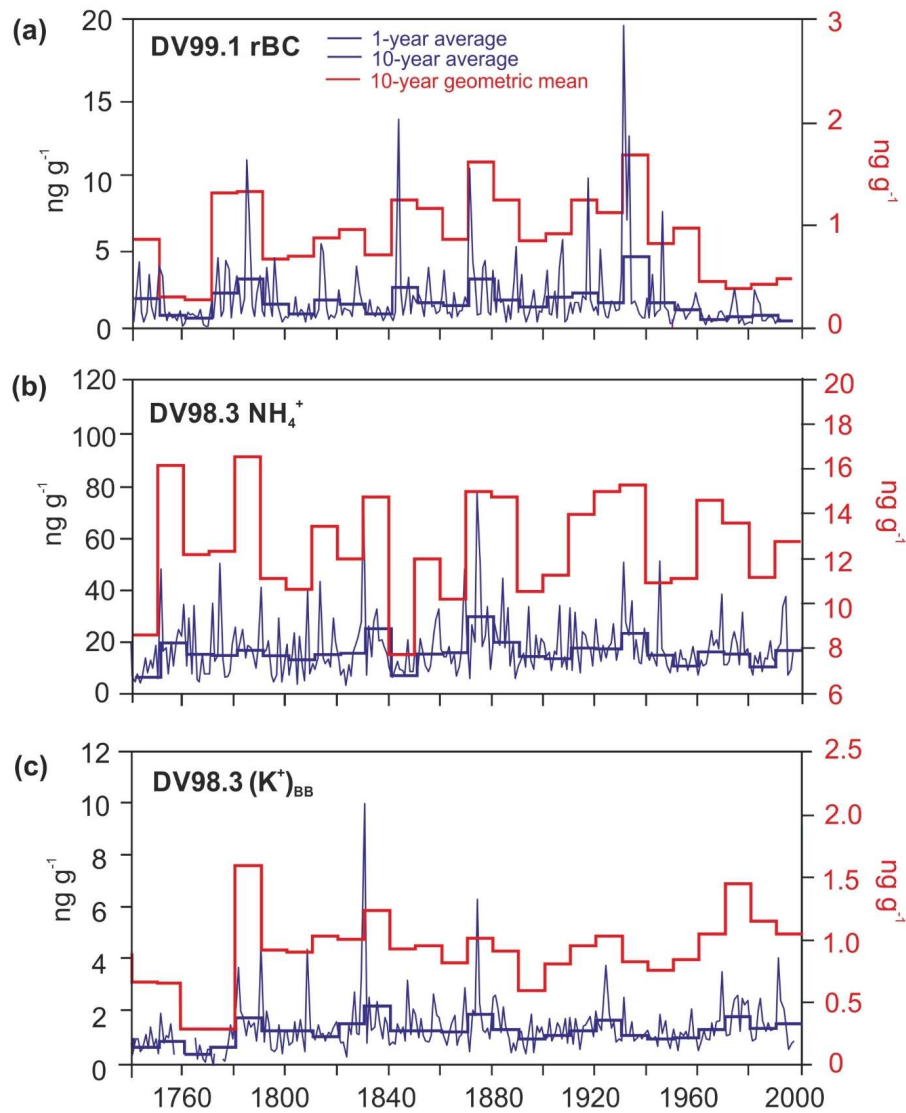


Figure S14. (a) rBC concentrations in the DV99.1 core, 1740-1992; (b) Ammonium (NH_4^+) and (c) the estimated biomass burning fraction of potassium ($(\text{K}^+)_{\text{BB}}$) in the DV98.1 core over the same time period. Two large outliers were removed from the $(\text{K}^+)_{\text{BB}}$ data. As in Fig. 4 in the paper, the blue lines represent \sim 1- and 10-year arithmetic averages of the data (scale at left), while the red stepped lines show the geometric mean of the data over 10-year intervals (scale at right).

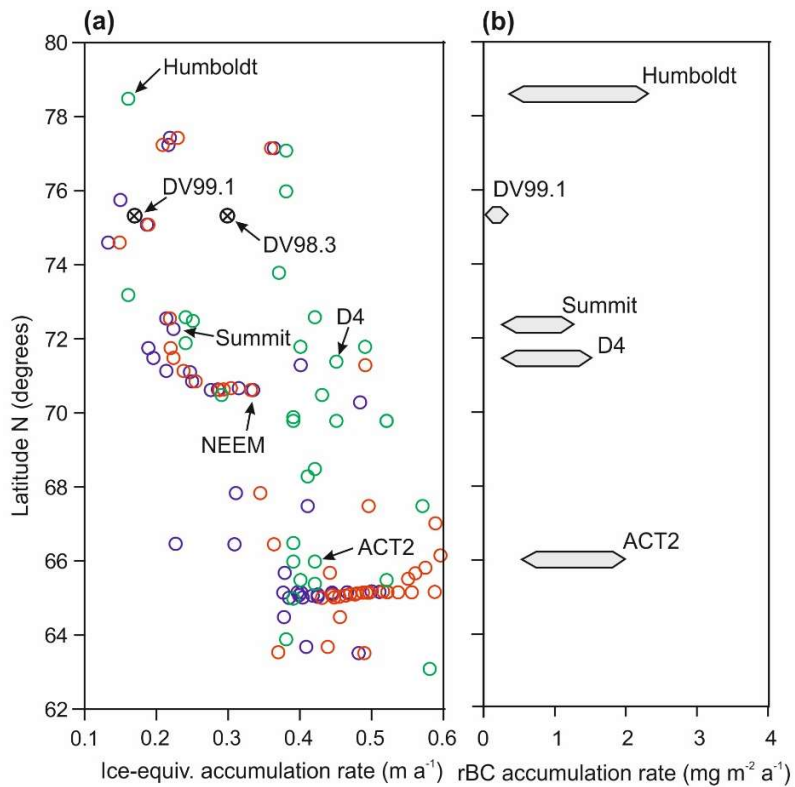


Figure S15. (a) Latitudinal variations in ice-equivalent mass accumulation rates across Greenland (62 to 80°), compared with estimates for sites DV98.3 and DV99.1 on Devon ice cap. Greenland data are from Bales et al. (2009), spanning 1960-69 (blue circles) and 1970-79 (red circles), and from Buchardt et al. (2012), spanning various periods between 1957 and 2003. **(b)** Compared ice-core based estimates of rBC net accumulation rates in snow in Greenland (Lee et al., 2013; sites shown on Fig. 5) and at site DV99.1 on Devon ice cap. Polygons depict ranges of values for the period between the early 1960s and late 1990s.

References

- Bales, R.C., Guo,Q., Shen, D., McConnell, J.R., Du,G., Burkhart, J.F., Spikes, V.B., Hanna, E. and Cappelen, J.: Annual accumulation for Greenland updated using ice core data developed during 2000–2006 and analysis of daily coastal meteorological data, *J. Geophys. Res.*, 114, D06116, doi:10.1029/2008JD011208, 2009.
- Buchardt, S. L., Clausen, H. B., Vinther, B. M. and Dahl-Jensen, D.: Investigating the past and recent ^{18}O -accumulation relationship seen in Greenland ice cores. *Clim. Past*, 8, 2053–2059, 2012.
- Lee, Y.H., Lamarque, J.F., Flanner, M.G., Jiao, C., Shindell, D.T., Berntsen, T., Bisiaux, M.M., Cao, J., Collins, W.J., Curran, M., Edwards, R., Faluvegi, G., Ghan, S., Horowitz, L.W., McConnell, J.R., Ming, J., Myhre, G., Nagashima, T., Naik, V., Rumbold, S.T., Skeie, R.B., Sudo, K., Takemura, T., Thevenon, F., Xu, B. and Yoon, J.-H.: Evaluation of preindustrial to present-day black carbon and its albedo forcing from Atmospheric Chemistry and Climate Model Intercomparison Project (ACCMIP). *Atmos. Chem. Phys.*, 13, 2607–2634, doi:10.5194/acp-13-2607-2013, 2013.
- McConnell, J. R. and Edwards, R.: Coal burning leaves toxic heavy metal legacy in the Arctic. *P. Natl. Acad. Sci. USA*, 105, 12,140–12,144, doi:10.1073/pnas.0803564105, 2008.
- McConnell, J. R., Edwards, R., Kok, G. L., Flanner, M. G., Zender, C. S., Saltzman, E. S., Banta, J. R., Pasteris, D. R., Carter, M. M., and Kahl, J.D.: 20th-century industrial black carbon emissions altered Arctic climate forcing. *Science*, 317, 1381–1384, doi:10.1126/science.1144856, 2007.